

Drawing tubular fibres: experiments versus mathematical modelling

Michael J. Chen,^{1*} Yvonne M. Stokes,¹ Peter Buchak,² Darren G. Crowdy,² Herbert T.C. Foo,³ Alastair Dowler⁴ and Heike Ebendorff-Heidepriem³

¹*School of Mathematical Sciences, The University of Adelaide, Adelaide, South Australia 5005, Australia*

²*Department of Mathematics, Imperial College London, 180 Queen's Gate, London, SW7 2AZ, UK*

³*ARC Centre of Excellence for Nanoscale BioPhotonics, Institute for Photonics and Advanced Sensing, School of Physical Sciences, The University of Adelaide, North Terrace, Adelaide, SA 5005, Australia*

⁴*Institute for Photonics and Advanced Sensing, School of Physical Sciences, The University of Adelaide, North Terrace, Adelaide, SA 5005, Australia*

[*michael.chen@adelaide.edu.au](mailto:michael.chen@adelaide.edu.au)

Abstract: A series of six experiments drawing tubular fibres are compared to some recent mathematical modelling of this fabrication process. The importance of fibre tension in determining the internal geometry of the fibre is demonstrated, confirming a key prediction of the models. There is evidence of self-pressurisation of the internal channel, where an additional pressure is induced in the internal channel as the fibre is drawn, and the dependence of the magnitude of this pressure on fibre tension is discussed. Additionally, there is evidence that the difference between the glass and furnace temperatures is proportional to the furnace temperature and dependent on the preform geometry.

© 2015 Optical Society of America

OCIS codes: (000.3870) Mathematics; (060.2280) Fiber design and fabrication; (060.2310) Fiber optics; (060.4005) Microstructured fibers.

References and links

1. Y. M. Stokes, P. Buchak, D. G. Crowdy, and H. Ebendorff-Heidepriem, "Drawing of micro-structured fibres: circular and non-circular tubes," *J. Fluid Mech.* **755**, 176–203 (2014).
2. P. Buchak, D. G. Crowdy, Y. M. Stokes, and H. Ebendorff-Heidepriem, "Elliptical pore regularization of the inverse problem for microstructure optical fibre fabrication," *J. Fluid Mech.* **778**, 5–38 (2015).
3. M. J. Chen, Y. M. Stokes, P. Buchak, D. G. Crowdy, and H. Ebendorff-Heidepriem, "Microstructured optical fibre drawing with active channel pressurisation," *J. Fluid Mech.* **783**, 137–165 (2015).
4. H. Tronnolone, Y. M. Stokes, H. T. C. Foo, and H. Ebendorff-Heidepriem, "Gravitational extension of a fluid cylinder with internal structure," *J. Fluid Mech.* **submitted** (2015).
5. T. M. Monro and H. Ebendorff-Heidepriem, "Progress in microstructured optical fibers," *Ann. Rev. Materials Res.* **36**, 467–495 (2006).
6. S. Xue, R. Tanner, G. Barton, R. Lwin, M. Large, and L. Poladian, "Fabrication of Microstructured Optical Fibres Part I: Problem Formulation and Numerical Modelling of Transient Draw Process," *J. Lightwave Technol.* **23**, 2245–2254 (2005).
7. G. Luzi, P. Epple, M. Scharrer, K. Fujimoto, C. Rauh, and A. Delgado, "Numerical Solution and Experimental Validation of the Drawing Process of Six-Hole Optical Fibers Including the Effects of Inner Pressure and Surface Tension," *J. Lightwave Technol.* **30**, 1306–1311 (2012).
8. G. T. Jason, J. S. Shrimpton, Y. Chen, T. Bradley, D. J. Richardson, and F. Poletti, "MicroStructure Element Method (MSEM): viscous flow model for the virtual draw of microstructured optical fibers," *Opt. Express* **23**, 312–329 (2015).

9. A. D. Fitt, K. Furusawa, T. M. Monro, and C. P. Please, "Modelling the Fabrication of Hollow Fibers: Capillary Drawing," *J. Lightwave Technol.* **19**, 1924–1931 (2001).
 10. A. D. Fitt, K. Furusawa, T. M. Monro, C. P. Please, and D. J. Richardson, "The mathematical modelling of capillary drawing for holey fibre manufacture," *Journal of Engineering Mathematics* **43**, 201–227 (2002).
 11. Y. Chen and T. Birks, "Predicting hole sizes after fibre drawing without knowing the viscosity," *Optical Materials Express* **3**, 346–356 (2013).
 12. A. L. Yarin, P. Gospodinov, and V. I. Roussinov, "Stability loss and sensitivity in hollow fiber drawing," *Phys Fluids* **6**, 1454–1463 (1994).
 13. P. Gospodinov and A. L. Yarin, "Draw resonance of optical microcapillaries in non-isothermal drawing," *Intl J. Multiphase Flow* **23**, 967–976 (1997).
 14. C. J. Joyce, A. D. Fitt, and T. M. Monro, "Mathematical Modeling as an Accurate Predictive Tool in Capillary and Microstructured Fiber Manufacture: The Effects of Preform Rotation," *J. Lightwave Technol.* **26**, 791–798 (2008).
 15. C. J. Joyce, A. D. Fitt, J. R. Hayes, and T. M. Monro, "Mathematical Modeling of the Self-Pressurizing Mechanism for Microstructured Fiber Drawing," *J. Lightwave Technol.* **27**, 871–878 (2009).
 16. R. Kostecki, H. Ebendorff-Heidepriem, S. C. Warren-Smith, and T. M. Monro, "Predicting the drawing conditions for microstructured optical fiber fabrication," *Optical Materials Express* **4**, 29–40 (2014).
 17. L. Cummings and P. Howell, "On the evolution of non-axisymmetric viscous fibres with surface tension, inertia and gravity," *Journal of Fluid Mechanics* **389**, 361–389 (1999).
 18. Schott Glass Company, *Optical Glass* (2014).
 19. M. Trabelssi, H. Ebendorff-Heidepriem, K. C. Richardson, T. M. Monro, and P. F. Joseph, "Computational modeling of die swell of extruded glass preforms at high viscosity," *J. Am. Ceram. Soc.* **97**, 1572–1581 (2014).
-

1. Introduction

We report on a series of experiments drawing tubular glass fibres which have been performed to test the validity of a recent model of this fabrication process [1]. The model of tubular fibres is part of a larger project to investigate the fabrication of microstructured optical fibres (or MOFs) with the techniques of mathematical modelling [1–4]. MOFs are distinguished from solid optical fibres by the cross-sectional structure running along their length. The design of this cross-sectional structure, which acts to change the refractive index from that of the pure glass, gives the fibre certain optical and physical properties which are desirous in a range of applications (see, for instance, [5]).

The fabrication process involves slowly feeding a preform of suitable geometry (typically 1–3 cm in diameter) into a heated region within a furnace and then stretching the softened glass to the dimensions of a fibre (typically external diameters of 120–250 μm and internal channel diameters in the order of the wavelength of light). Modelling is required to determine how the preform geometry deforms as it is drawn to fibre.

Recent modelling by some of the current authors [1–3] has considerably advanced understanding of how the internal structures in MOFs deform during fabrication. In particular, it has been established that the competition between the stretching of the fibre and surface tension on the internal channels ultimately determines the shape and pattern of channels in the fibre that results from a given preform design and a choice of operating parameters [1]. This is true for any preform design and sophisticated mathematical techniques have been developed to describe the geometry deformation for a class of optically important MOFs [2]. An extra degree of control on the deformation of the geometry may be achieved by applying an overpressure to the internal channels as the fibre is drawn and this potentially allows a greater variety of internal fibre geometries to be achieved [3]. Three-dimensional finite element simulations of fibre drawing have been performed by others for MOFs with up to 6 channels [6, 7]. Our approach of [1–3] is much more computationally efficient especially for MOF designs with many channels, which may not be feasible with 3D finite element simulations. MOFs of a specific class have recently been modelled with a focus on computational efficiency [8] by assuming that the channels are separated by thin walls, whereas our approach makes no such assumption and can therefore MOF treat designs more generally.

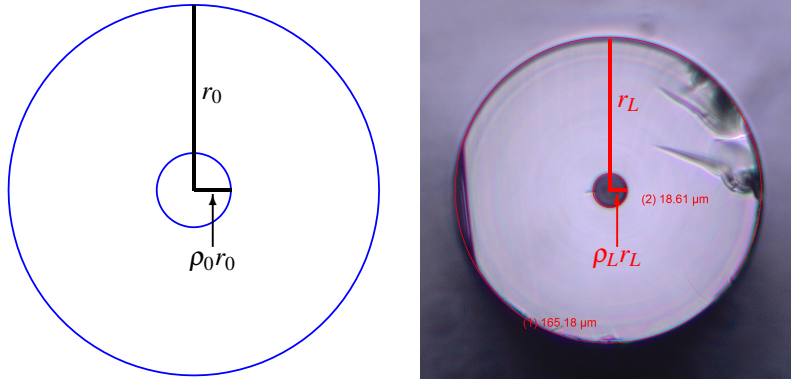


Fig. 1. A schematic diagram of an annular preform (left) and a microscope image of a drawn tubular fibre (right). The outer radius of the preform is denoted r_0 and the radius of the fibre is r_L . The ratio between the inner and outer radii of the preform is ρ_0 and the ratio between the inner and outer radii of the fibre is ρ_L .

The annular tubes described in the current paper are the simplest fibre design containing internal structure and gaining understanding of the fabrication process for this simple case is a useful test of the modelling approach. This will serve as a guide to later experiments which will focus on more complex fibre designs with multiple channels to validate the more sophisticated modelling required for those cases [1, 2].

Previous studies on tubular fibres have compared a model with experiments [9, 10], but did not consider the role of fibre tension since the importance of this quantity has only recently been understood [1, 11]. Stability considerations in fibre-drawing theoretically restrict the choice of operating conditions [12, 13], although the destabilising phenomenon of ‘draw resonance’ reported in the literature is not present in the current experiments. Further studies have investigated the role of additional effects via theory and experiments. Rapid rotation of the preform during the draw may be used to exert control over the geometry [14], for instance, and modelling has been used to investigate the utility of the practice of sealing the ends of the preform to prevent channel closure [15].

The models for drawing tubular fibres with and without active channel pressurisation (from [1] and [3], respectively) are given in Section 2. Details of the experimental materials, apparatus and procedures are given in Section 3. Section 4 summarises the results of the six experiments and compares this data with the model output, including discussions on the role of self-pressurisation and furnace temperature. Our conclusions are presented in Section 5.

2. Mathematical model for drawing annular MOFs

As shown in the schematic diagram in Fig. 1, the ratio of the radii of the inner and outer boundaries in the preform is denoted ρ_0 and the ratio of these radii in the fibre is ρ_L . The preform is fed into the heated neck-down region with feed speed U_0 and is drawn off at the end of this region with draw speed U_L . The ratio of these two speeds D is the draw ratio and, by conservation of mass, this is also the ratio of the preform and fibre areas, so that

$$D = U_L/U_0 = S_0/S_L, \quad (1)$$

where S_0 is the cross-sectional area of the preform and S_L is the area of the fibre.

As established in our modelling work [1–3] and in [11], the tension in the fibre is a key

quantity in predicting the change in the geometric structure between the preform and the fibre. Validating this relationship with experiments is the principle aim of this paper. The fibre tension σ is a measurable quantity on current fibre drawing equipment and we introduce a dimensionless fibre tension parameter \mathcal{T} , for convenience of mathematical modelling; these are related via

$$\sigma = 6\gamma\sqrt{S_0}\mathcal{T}, \quad (2)$$

where γ is the surface tension. Similarly μ_0 is the harmonic mean of the viscosity over the length L of the neck-down region over which the change in geometry occurs, and is related to a dimensionless parameter \mathcal{M} where

$$\frac{\mu_0}{L} = \frac{\gamma}{U_0\sqrt{S_0}}\mathcal{M}. \quad (3)$$

The neck-down zone corresponds to a region near the peak of Kostecki's temperature profiles [16] where the temperature of the glass is such that its viscosity is low enough to be malleable. Note that the temperature profile of the glass differs from the furnace profile because of the imperfect transfer of radiative heat to a semi-transparent material like glass.

The modelling work of [1] and [3] introduced additional parameters for mathematical convenience to describe the annular geometry of the preform and the fibre. These are derived from the ratio of the inner and outer boundaries and are given by

$$\alpha_0 = \alpha(\rho_0), \quad \alpha_L = \alpha(\rho_L), \quad \text{where } \alpha(\rho) = \frac{1}{\sqrt{\pi}}\sqrt{\frac{1-\rho}{1+\rho}}. \quad (4)$$

In practice, we apply our model by starting with a ρ_0 value (known or measured from the preform) and convert this to α_0 via Eq. (4) for the purposes of the model. The model output for a set of drawing parameters (namely D and \mathcal{T}) is then obtained in terms of α_L , see sections 2.1 and 2.2 below, which may then be converted to the more easily interpretable quantity ρ_L via a rearrangement of Eq. (4), namely

$$\rho_L = \frac{1 - \pi\alpha_L^2}{1 + \pi\alpha_L^2}. \quad (5)$$

An additional quantity of interest is the outer radius of the fibre r_L , which may be written in terms of the other parameters as

$$r_L = \sqrt{\frac{S_0}{\pi D(1-\rho_L^2)}} = r_0\sqrt{\frac{1-\rho_0^2}{D(1-\rho_L^2)}}, \quad (6)$$

where r_0 is the outer radius of the preform, and $S_0 = \pi r_0^2(1-\rho_0^2)$. The inner radius of the fibre is then $\rho_L r_L$.

The model also determines \mathcal{M} and so gives μ_0 the harmonic mean of viscosity in the glass from Eq. (3) for a given neck-down length L . This may then be used to calculate the temperature in the glass T_{glass} ($^{\circ}\text{C}$) corresponding to μ_0 via a temperature-viscosity relation, provided this is known for a particular glass.

2.1. Summary of model for drawing tubular fibres without active pressurisation

We now briefly summarise some key results from [1] which, among general results, presents a complete analytic solution for the drawing of annular fibres (see section 4 of that work for full

details). The modelling approach developed in that paper is extremely general and can, in fact, deal with the complex cross-sectional design of a MOF (which features many holes) not just the simplest possible holey structure of an annular fibre.

As stated above, for the purposes of this paper it is sufficient to consider the output of the model as simply the fibre geometry parameter α_L for a given draw ratio D and dimensionless tension parameter \mathcal{T} . It is straightforward to apply the model from [1] to evaluate α_L in this way, as well as determine the additional parameter \mathcal{M} for the viscosity of the glass (and the corresponding temperature in the glass). The cross-sectional area S and geometry parameter α at any position along the neck-down are related by

$$\sqrt{\frac{S}{S_0}} = \left(\frac{\alpha}{\alpha_0}\right)^{1/3} (1 + 3\alpha_0\mathcal{T}) - 3\alpha_0\mathcal{T} \left(\frac{\alpha}{\alpha_0}\right). \quad (7)$$

Then at the fibre end of the neck-down, where $\alpha = \alpha_L$ and $S = S_L = S_0/D$, we obtain after a little rearrangement

$$\left(\frac{\alpha_L}{\alpha_0}\right) - \left(\frac{\alpha_L}{\alpha_0}\right)^{1/3} \left(\frac{1}{3\alpha_0\mathcal{T}} + 1\right) + \frac{1}{\sqrt{D}} \frac{1}{3\alpha_0\mathcal{T}} = 0, \quad (8)$$

which is a cubic polynomial in $(\alpha_L/\alpha_0)^{1/3}$. It is straightforward to find the relevant root of Eq. (8). In practice, we find it more convenient to evaluate the roots of the cubic numerically (in MATLAB, for instance), but if desired α_L may be expressed as a closed form solution, namely

$$\alpha_L = \frac{8\alpha_0}{3\sqrt{3}} \left(\frac{1}{3\alpha_0\mathcal{T}} + 1\right)^{3/2} \cos^3 \frac{\theta}{3}, \quad (9)$$

with

$$\theta = \arctan \left(-\sqrt{\frac{4D}{27} \frac{(1 + 3\alpha_0\mathcal{T})^3}{3\alpha_0\mathcal{T}} - 1} \right) + \pi. \quad (10)$$

An alternate expression for α_L may be derived via a series expansion assuming, as in fibre drawing, that $\sqrt{D} \gg 1$, and then performing a perturbation expansion on Eq. (8). The first two terms of the resulting series are an excellent approximation to the relevant exact root of that equation and the resulting expression for α_L is

$$\alpha_L \approx \alpha_0 \left(\sqrt{1 + \frac{1}{3\alpha_0\mathcal{T}}} - \frac{1}{2\sqrt{D}} \frac{1}{1 + 3\alpha_0\mathcal{T}} + \dots \right)^3. \quad (11)$$

Once α_L has been found it is possible to calculate the remaining parameter \mathcal{M} , as given in [1] (note that $\mathcal{M} \equiv 1/(M\gamma^*)$ in the notation of that paper, where M is the inverse harmonic mean of dimensionless glass viscosity over the neck down region). The relevant expression for that parameter is

$$\mathcal{M} = \frac{\mathcal{T}}{\log Q}, \quad \text{with } Q = \sqrt{D} \left(\frac{\alpha_L}{\alpha_0}\right)^{1/3}, \quad (12)$$

and this value for \mathcal{M} is substituted into Eq. (3) to obtain the harmonic mean of the dimensional glass viscosity μ_0 .

2.2. Summary of model for drawing tubular fibres with active pressurisation

As detailed in [3], including active pressurisation of the internal channels changes the mathematical structure of the fibre drawing model, as compared to the unpressurised model of [1]. This means that for tubular fibres, there is no longer an exact solution of the type presented above, rather it is necessary to solve a system of differential equations to determine α_L numerically.

The applied pressure in the internal channel is denoted as p_H . A dimensionless pressure parameter \mathcal{P} is introduced and this is related to the dimensional pressure by

$$p_H = \frac{\gamma}{\sqrt{S_0}} \mathcal{P}. \quad (13)$$

Full details of the derivation of the following equations are given in [3], along with a complete discussion of various more mathematical aspects of the pressurised model. The fibre geometry parameter α_L is found by the simultaneous solution of the differential equations

$$\frac{d\alpha}{d\tau} = \frac{1}{2} - \frac{1}{8\pi\alpha} (1 - \pi^2\alpha^4) \mathcal{P}\chi, \quad (14)$$

$$\frac{d\chi}{d\tau} = \frac{1}{6} \frac{\chi}{\alpha} - \mathcal{T}, \quad (15)$$

where these equations are integrated forward in the independent variable τ from $\chi = 1$ to $\chi = 1/\sqrt{D}$, where $\chi = \sqrt{S/S_0}$ is the square root of the scaled cross-sectional area as it varies from preform to the fibre, such that at the top of the neck-down region $\chi = 1$ (preform) and at the bottom of the neck-down region $\chi = 1/\sqrt{D}$. The independent variable τ in the above equations is the ‘reduced time’ first introduced for fibre drawing by [17], which measures the time since the start of deformation of the cross-section (accounting for the scaling of the problem and a varying viscosity) from $\tau = 0$ to $\tau = \tau_L$, and is, therefore, also a measure of the distance travelled along the neck-down length from $x = 0$ to $x = L$. To determine the fibre geometry parameter α_L we solve Eqs. (14)–(15) from $\chi = 1$ to $\chi = 1/\sqrt{D}$ with the initial condition $\alpha(\chi = 1) = \alpha_0$, representing the preform geometry at the top of the neck down region. The final geometry is thus $\alpha(\chi = 1/\sqrt{D}) = \alpha_L$.

When performing pressurised fibre drawing care must be taken not to apply too much pressure or the fibre may catastrophically explode. An approximate criterion on the pressurisation parameter \mathcal{P} was proposed in [3] for fibre explosion (so this may be avoided), that explosion occurs if

$$\mathcal{P} > \frac{8\pi}{3} \alpha_0 (3\mathcal{T}\alpha_0 + 1). \quad (16)$$

Similarly, there is a possibility that the central channel will deform in the drawing process to the point that it closes completely (typically this happens for low fibre tension). As described in [3], this hole closure occurs if

$$\mathcal{P} < \frac{a^2\sqrt{D}}{9(D-1)} \left(a(\alpha_0 - 1/\sqrt{\pi}) + 3(\sqrt{D} - 1) \right) + \frac{2}{3}\pi\sqrt{D} \left(1 + 3\frac{\sqrt{D}}{\sqrt{\pi}} \mathcal{T} \right), \quad (17)$$

with $a = -\sqrt{\pi} + 6\mathcal{T}\sqrt{D}$. As discussed in detail in [3], the explosion criterion in Eq. (16) is preferable to a similar criterion given in [10]. Equation (16) predicts explosion for a higher value of pressure than that predicted by the criterion in [10], which in turn permits fibres with a larger ρ_L (that is, with thinner walls) to be drawn with confidence. Similarly, the closure criterion in Eq. (17) is preferable to the version in [10]. The modelling in [3] indicated that the

Table 1. Summary of the dimensions of the preform and the operational parameter values used in the six experiments. Additionally, the surface tension parameter for F2 glass, which was used in all the above experiments, is $\gamma = 0.23\text{Nm}^{-1}$ and the neck down length was approximately $L = 0.03\text{m}$. The numbers in brackets which follow the ranges for T_{furnace} , U_{draw} and p_H indicate the number of incremental steps taken to vary these operational parameters between the stated values during the course of a given experiment.

Experiment	Preform dimensions		Operational parameters			
	ρ_0	$2r_0$ (mm)	U_{feed} (mm/min)	U_{draw} (m/min)	T_{furnace} (°C)	p_H (Pa)
1	0.16	10.33–10.14	1.4	5.8	940–880 (6)	0
2	0.16	10.92–10.66	1.4	6.1	940–905 (4)	0
3	0.515	10.39–10.49	1.39	7.4	985–955 (4)	0
4	0.514	10.31–10.21	1.4	5.9	980–950 (4)	0
5	0.168	10.50–10.24	1.4	2.2–12 (6)	930	0
6	0.17	10.54–10.33	1.4	5.6	900	0–3000 (4)

critical value of pressure given by Eq. (17) corresponds to a fibre with a very small diameter internal channel; crucially the channel is not fully closed at this predicted pressure value. The criterion in [10], however, predicts a smaller value of pressure and when used in the model of [3] this pressure was insufficient to prevent hole closure.

3. Experimental materials and procedure

The experiments were performed with F2 glass, a commercially available lead-silicate soft glass by the Schott Glass Company [18]. This glass is ideal for prototyping MOF designs and validating models of fabrication since it is an excellent, less expensive analogue for pure silica glass, which is more commonly used in MOF fabrication. The two glasses have near identical surface tension and display a similar rate of change in viscosity during heating and cooling. The surface tension for F2 glass is $\gamma = 0.23\text{Nm}^{-1}$ [1]. A Vogel-Fulcher-Tammann temperature-viscosity relation for F2 glass is given in [1], and is

$$T_{\text{glass}} = 137 + \frac{4065.2}{\log_{10} \mu_0 + 2.314}. \quad (18)$$

Using a similar setup to that described in [16], we have measured the temperature profile inside the furnace used for these F2 glass drawing experiments. These measurements demonstrated that T_{glass} is approximately 200–300°C lower than the furnace temperature.

Six tubular preforms were manufactured by extruding F2 glass through a suitably designed die. Two die designs were used, one where the ratio between the inner and outer die boundaries was 0.2 (used for experiments 1, 2, 5 and 6) and another where this ratio was 0.6 (used for experiments 3 and 4). The resulting tubular preforms have a ratio of inner and outer diameters ρ_0 slightly less than that of the die, due to the effects of die swell [19], gravity stretching and surface tension as the softened glass is extruded and cools; this is similar to the deformation seen in fibre drawing, and modelling of the stretching that occurs during the extrusion process is ongoing, see for instance [4]. Additionally, the gravity stretching and other non-uniformities during the extrusion process result in preforms which vary slightly in outer diameter along their length, and we describe how to account for this variation in Section 4.1. Once cooled, a preform is cut into sections approximately 18 cm long and it is these shorter preforms which are drawn to fibre.

Fibre drawing was performed on the 4 m soft glass drawing tower at the Institute of Photonics and Advanced Sensing (IPAS) at the University of Adelaide. This tower has the ability to measure quantities such as fibre diameter and fibre tension in real-time; the latter is crucial in validating the modelling approach. The preforms were held in a chuck connected to a hollow feed tube allowing the preform to be slowly lowered into the furnace. The top of the feed tube, and therefore the top of the preform, was open to the atmosphere. Each of the six preforms were drawn to 200–300 m of fibre and the operational parameters used in each experiment, namely the feed speed U_{feed} , the draw speed U_{draw} , the furnace temperature T_{furnace} and the active pressurisation p_H , are given in Table 1. In each experiment one of these operational parameters was systematically varied to determine its effect on the properties of the resulting fibre, while the other parameters were fixed. In Table 1 the minimum and maximum of the parameter that varied in each experiment is given. The number of incremental steps taken to vary a parameter between these minimum and maximum values is given in brackets after the relevant range in Table 1. For instance, in experiment 1 the furnace temperature was varied from 940°C to 880°C in six increments. After each change of an operational parameter the fibre was drawn for at least five minutes so it had reached a steady state.

For each experiment, as the draw progressed the lengths of the fibre corresponding to a given choice of parameters within each experiment were divided into separate bands as they were wound round the drum. Five to nine samples were taken from within each band of fibre and the inner and outer diameters of each sample were measured using an optical microscope, from which the fibre diameter ratio ρ_L was calculated. The values given in Section 4.2 below are an average of these measurements. The measurement error of ρ_L is approximately 5%, as indicated by the error bars on each data point in the plots in Section 4.2. Additionally, the measurement error on the inner and outer fibre diameters is ± 2 microns, the error on the tension is ± 2 g, the error on U_{draw} is ± 0.1 m/min and the error on the applied pressure is ± 10 Pa.

4. Experimental results and model validation

The properties of the six preforms, as well as the parameters used for each experiment are summarised in Table 1. Experiments 1 and 2 involved drawing preforms with a geometry of $\rho_0 = 0.16$ over a range of furnace temperatures. Experiments 3 and 4 were also drawn over a range of furnace temperatures, but used preforms with a larger internal channel; their geometries were $\rho_0 = 0.515$ and $\rho_0 = 0.514$, respectively. In these four experiments, as the furnace temperature (and therefore glass temperature) is decreased the tension in the fibre increases. The effect of varying fibre tension σ on the fibre diameter ratio is the key point of interest in this study, since an important implication of the modelling work [1, 3] is that fibre tension determines the geometry deformation between preform and fibre. Knowledge of fibre tension, which is measurable during the draw on current equipment, obviates the need to know about glass temperature and neck-down length which are impossible to measure during a fibre draw.

Experiment 5 used a preform of similar internal geometry to the first two experiments, with $\rho_0 = 0.168$, but varied the draw speed U_d while keeping the furnace temperature fixed. Experiment 6 involved drawing a preform with $\rho_0 = 0.17$ over a range of active pressurisations. This last experiment aims to validate the model for annular fibres drawn under active pressurisation [3], as summarised in Section 2.2.

4.1. Accounting for preform taper

As described in section 3, each preform was produced by extruding softened glass through a purpose-designed die. Extruded preforms typically exhibit a taper in their outer diameter since the softened glass emerging from the die exit is stretched by the weight of the already extruded glass due to gravity. This variation in each of the six preforms, as measured prior to

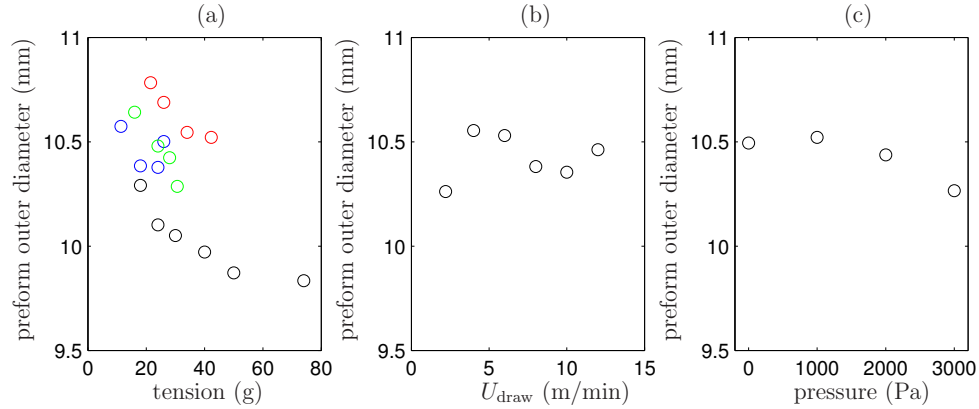


Fig. 2. The preform outer diameter $2r_0$ shows taper and was calculated for the six experiments using Eq. (19). Figure 2(a) shows the calculated preform outer diameter versus fibre tension for experiments 1 (black), 2 (red), 3 (blue) and 4 (green). Figure 2(b) shows the calculated preform outer diameter versus draw speed for experiment 5. Figure 2(c) shows the calculated preform outer diameter versus applied pressure for experiment 6.

the experiments, is indicated by the range of values given for the preform diameter $2r_0$ in Table 1. The first number in the stated range corresponds to the part of the preform lowered into the furnace first. For all but experiment 3 the thickest part of the preform was drawn to fibre first.

In the model the diameter of the fibre is very sensitive to the diameter of the preform, see Eq. (6). Thus, to compare the model with an experimental result it is necessary to use in the model the diameter of that part of the preform that gave rise to the portion of the fibre from which the experimental result was obtained. In practice, it is not possible to know the exact preform diameter that corresponds with a given point along the length of the fibre, meaning that it is necessary to somehow establish the appropriate values of $2r_0$ and S_0 that are associated with each experimental result. As described below, for each fibre cross-section of interest we use measurements of the fibre together with the draw ratio to calculate the diameter $2r_0$ of the corresponding preform cross-section.

The ratio of inner and outer boundaries of the tube ρ_0 is constant within the measurement error along the length of the preform, even as the preform outer boundary varies in radius; note that the pieces cut from the same extruded preform have identical ρ_0 (experiments 1 and 2) or vary by a small amount (less than 2% for experiments 3 and 4). Since $S_0 = \pi r_0^2 (1 - \rho_0^2)$, $S_L = \pi r_L^2 (1 - \rho_L^2)$ and $D = S_0/S_L$, the preform diameter is

$$2r_0 = 2r_L \sqrt{D} \sqrt{\frac{1 - \rho_L^2}{1 - \rho_0^2}}, \quad (19)$$

where (as stated) the fibre radius r_L and diameter ratio ρ_L have been measured and the draw ratio D is known, as is the preform diameter ratio ρ_0 . The computed preform diameters $2r_0$ for each experimental cross-section are displayed in Fig. 2. Figure 2(a) is for the four experiments in which the fibre tension was varied by changing the temperature, while all other draw parameters were fixed, so that the preform diameter is plotted against the tension used to draw that part of the preform into fibre. Similarly Fig. 2(b) is for the experiment in which the draw speed was varied and Fig. 2(c) is for that in which the pressure was varied. As can be seen in Figs. 2(a)–(c), the variation in radius of the preforms is, at most, less than 0.3mm. Although this is a relatively small variation in the preform it is important to take this into account when comparing the

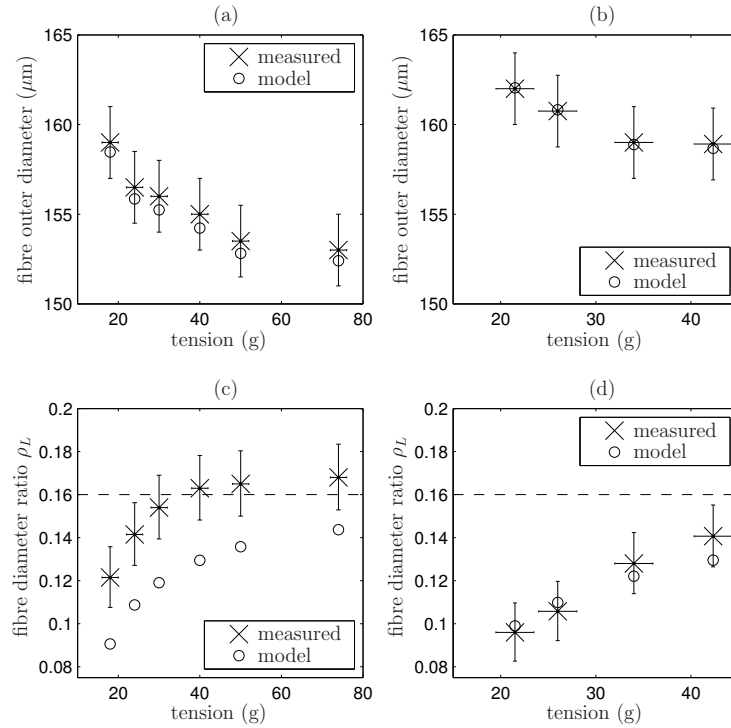


Fig. 3. Comparison between experimental measurements (crosses) and model output (circles) for experiments 1 and 2. Figures 3(a) and (c) show the outer diameter and the fibre diameter ratio, respectively, versus tension for experiment 1. Figures 3(b) and (d) show the outer diameter and fibre diameter ratio for experiment 2. The dashed lines in Figs. 3(c) and (d) represent the preform diameter ratio.

model output to the experiments, since fibre radius, as modelled by Eq. (6), is highly sensitive to small variations in the preform. Note that in Eqs. (2), (3), (6) and (13) the computed preform area $S_0 = DS_L = D\pi r_L^2 (1 - \rho_L^2)$ should be used.

4.2. Comparison of fibre diameter and geometry with model predictions

The properties of the measured fibres for the six experiments are shown against the model predictions in Figs 3–6, where each set of figures for the various experiments compare the measured outer diameter and fibre diameter ratio with the modelling. Experiments 1–5 are modelled as outlined in Section 2.1 and experiment 6, where a range of active pressurisations are applied to the preform, is modelled by solving the differential equations given in Section 2.2. Recall that a large value of the fibre diameter ratio ρ_L corresponds to a fibre with thin walls and conversely a small value of ρ_L corresponds to a fibre with thick walls.

The fibre measurements for experiments 1 and 2 are shown in Fig. 3. There is an excellent match between the predicted and observed outer diameter for both these experiments; within the measurement errors, all the measured outer diameters agree with the outer diameters predicted by our model. For experiment 1 the fibre diameter ratio ρ_L is consistently underestimated by the model, although the trend of the model as tension varies is in line with the experimental observations. The model predictions for ρ_L are in excellent agreement with the measured values for experiment 2, where the predicted values all lie within the measurement error of the

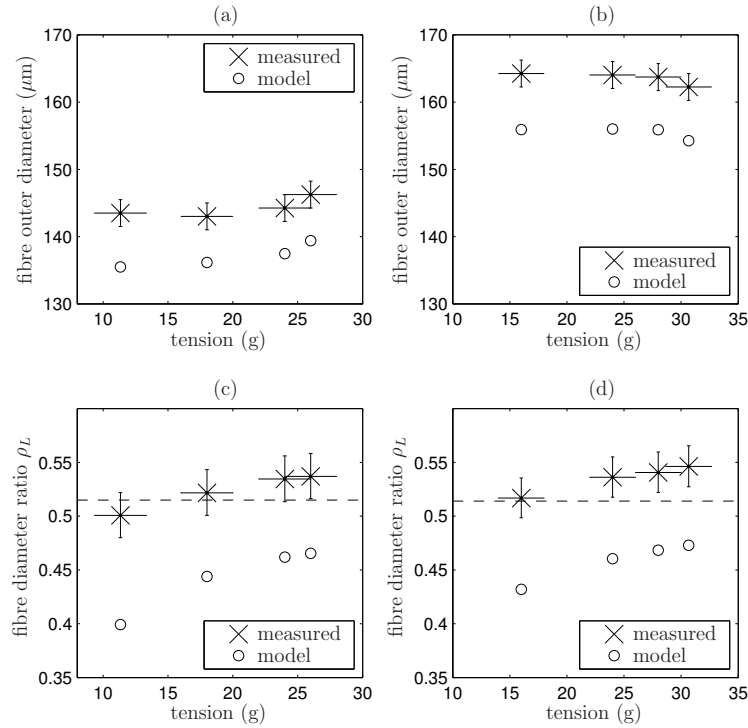


Fig. 4. Comparison between experimental measurements (crosses) and model output (circles) for experiments 3 and 4. Figures 4(a) and (c) show the outer diameter and the fibre diameter ratio, respectively, versus fibre tension for experiment 3. Figures 4(b) and (d) show the outer diameter and fibre diameter ratio for experiment 4. The dashed lines in Figs. 4(c) and (d) represent the preform diameter ratio.

observations.

Note that for the four largest fibre tensions shown in Fig. 3(c) the fibre diameter ratio ρ_L obtained in the experiment is within measurement error of the preform diameter ratio ρ_0 . This strongly implies that it is not surface tension alone acting to deform the geometry, since surface tension may only shrink the diameter ratio between preform and fibre. This suggests that another physical effect is present in the experiment but not accounted for in the model. Pressurisation is a likely candidate to explain the observed expansion of the geometry, and this will be discussed in more detail in Section 4.3.

The fibre measurements for experiments 3 and 4, which used preforms with a larger ρ_0 , are shown in Fig. 4. The model underestimates the outer diameter and ρ_L for both these experiments, with the model predictions falling well outside the measurement error. As in experiment 1 there is a systematic discrepancy between the observations and the model, with the outer diameter approximately $10\mu\text{m}$ smaller than the observations and ρ_L exhibiting the correct (upward) trend as tension is increased. Again, this apparently systematic discrepancy suggests that an effect is missing from the model. There is a larger difference here than in experiment 1 and this would be consistent with an induced pressurisation effect, since such an effect would have a relatively more severe impact on a larger diameter internal channel where the radius of curvature is larger and therefore the effect of surface tension is weaker.

The preform for experiment 5, which varied draw speed, was of similar dimensions to those

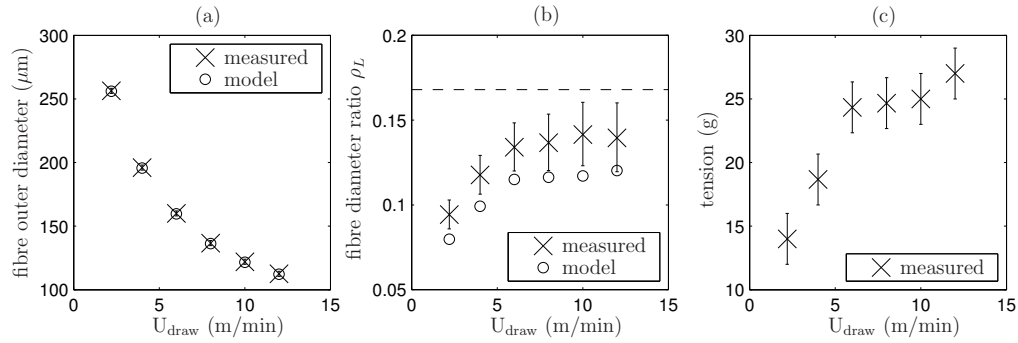


Fig. 5. Comparison between experimental measurements (crosses) and model output (circles) for experiment 5. Figure 5(a)–(b) show the outer diameter and the fibre diameter ratio, respectively, versus draw speed, with the preform diameter ratio shown as a dashed line in Fig. 5(b). Figure 5(c) shows the relationship between draw speed and the measured fibre tension. Note that the measurement error (not shown) on U_{draw} is ± 0.1 m/min.

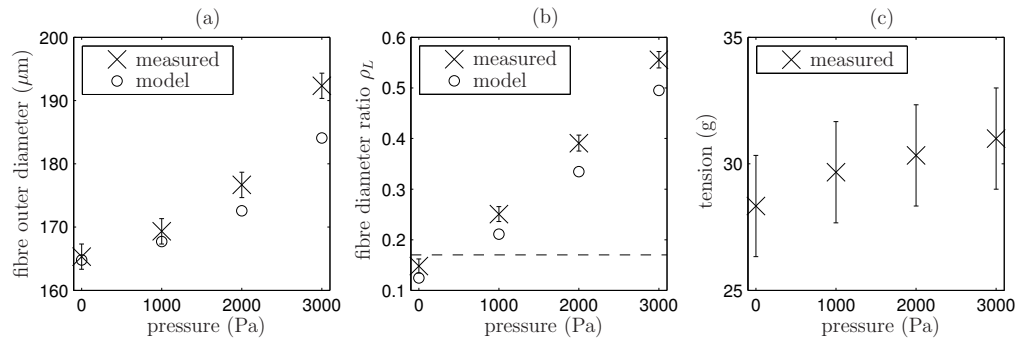


Fig. 6. Comparison between experimental measurements (crosses) and model (circles) output for experiment 6. Figures 6(a)–(b) show the outer diameter and the fibre diameter ratio, respectively, versus the applied channel pressurisation, with the preform diameter ratio shown as a dashed line in Fig. 6(b). Figure 6(c) shows the relationship between pressurisation and the measured fibre tension. Note that the measurement error (not shown) on the pressurisation is ± 10 Pa.

used in experiments 1 and 2. The fibre measurements for this experiment are compared to the model in Fig. 5, where these results are shown against draw speed. There is excellent agreement between the model and the outer diameter measurements, but ρ_L is consistently underestimated by the model. This discrepancy in ρ_L is extremely similar to the results of experiment 1 (Fig. 3c). Note that the differences between the model predictions and measurements of the fibre outer diameter in Fig. 5(a) are actually of a similar size to those in Fig. 3(a), but are obscured here due to the much larger range of diameters on the vertical axis. Fibre tension was measured throughout the draw and increased with draw speed, as shown in Fig. 5(c).

The fibre measurements for the pressurised experiment 6 are shown in Fig. 6. The draw was initially run without any active pressurisation, before the three successively larger pressures were applied. There is generally good agreement between all the measurements and the predicted values, especially given that ρ_L varies over a much larger range here than in the previous experiments. A few points fall outside the measurement error, again with some apparently systematic underestimation of ρ_L , but the trend as pressure is increased is in clear agreement with

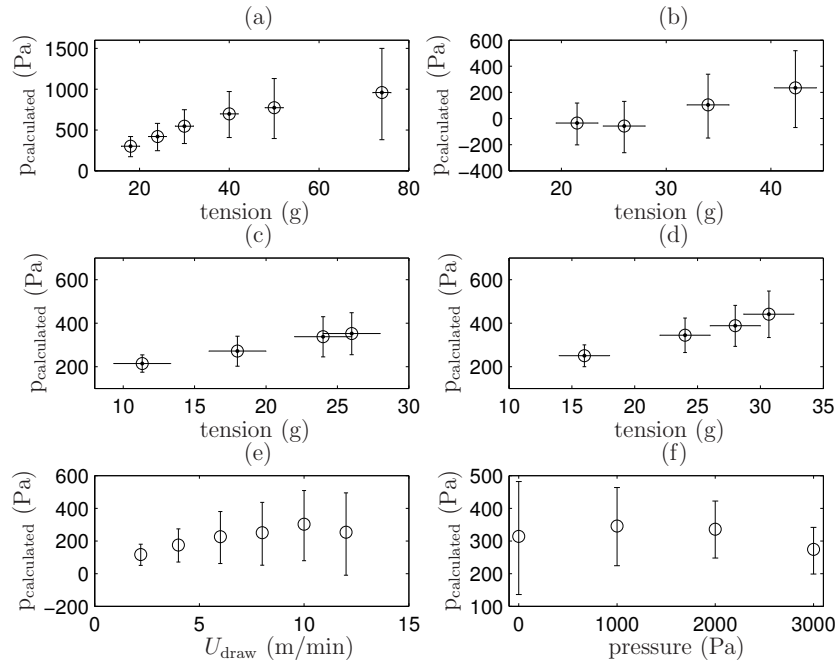


Fig. 7. Calculated pressurisation required for the model to exactly match the experimental data. Figures 7(a)–(d) are for experiments 1–4 and show the calculated pressure versus fibre tension. Figure 7(e) shows the calculated pressure for experiment 5 versus draw speed. Figure 7(f) shows the difference between calculated pressure and the applied pressure for experiment 6 versus the applied channel pressurisation.

the predictions of the model. The measured fibre tension increases slightly as the pressurisation is increased, as shown in Fig. 6(c).

4.3. Evidence of self-pressurisation

In several of the above model comparisons, in particular for experiments 1, 3, 4 and 5, the model underestimates the measured fibre diameter ratio ρ_L , see Figs. 3(c), 4(c)–(d) and 5(b), respectively. The consistent discrepancy between the modelling and the observations suggests that there is a physical effect present in the experiments that is not currently accounted for in the model. As noted above, a few of the observed ρ_L values are larger than the preform geometry ρ_0 which is not possible if the deformation is due to surface tension alone, since that effect acts to close the holes. A likely candidate is an induced pressurisation due to the change in geometry as the fibre is drawn, similar to the ‘self-pressurisation’ effect described by Voyce et al. [15]. In that work, the preform was sealed to the atmosphere and a pressure was induced due to the change in the total volume of air enclosed in the internal channel as the fibre is drawn. Note that for our experiments, the tubular preforms were open to the atmosphere.

The magnitude of pressure required to exactly match the data is determined by applying the pressurised annular fibre drawing model of [3], as given in section 2.2. This model is used in conjunction with an iterative bisection scheme to determine the exact value of pressurisation p_H required to match the observations at each choice of operational parameters. This pressure $p_{\text{calculated}}$ is found for each observation in the six experiments and the results are shown in Fig. 7. As shown in Figs. 7(a)–(d), in experiments 1–4, where furnace temperature (and therefore fibre

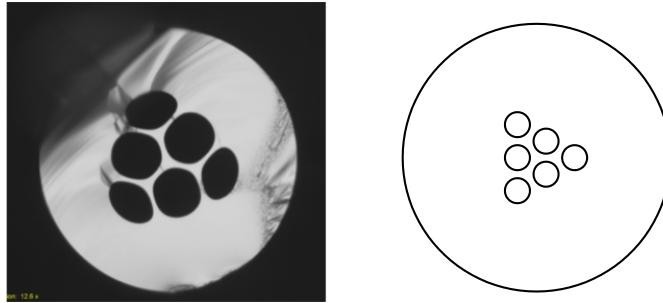


Fig. 8. A microscope image showing the cross-section of a fibre from a recent experiment (left) and a schematic of the preform from which it was drawn (right). Note that the relative sizes of the holes in the fibre are larger than those in the preform. Since this fibre was produced from an unpressurised draw, this is further evidence of self-pressurisation.

tension) was varied, the magnitude of the calculated pressure required to match the observations increases with fibre tension. Similarly, in experiment 5 the calculated pressure increases with draw speed; as shown in Fig. 5(c), fibre tension increases with draw speed, so this trend is consistent with the experiments which explicitly varied fibre tension. These calculated pressures are strong evidence that the accuracy of the model would be much improved by including a self-pressurisation effect. Establishing how this effect varies with the operational parameters requires further investigation and modelling. One hypothesis, suggested by Fig. 7, is that the magnitude of the self-pressurisation is proportional to the fibre tension.

The calculated pressures for Experiment 6, which was actively pressurised, are shown in Fig. 7(f) as the difference between the applied and calculated pressures for each observation. Rather than being evidence of self-pressurisation, this may indicate that there is a discrepancy between the pressure as measured by the drawing tower and the pressure actually applied to the preform. This is not unexpected since the draw tower measures pressure in a hose some distance away from the preform. For $p_H = 0\text{--}3000$ Pa there is approximately a 300 Pa difference, which is similar to the pressure offset suggested by other authors [16].

Self-pressurisation is also observed experimentally in drawing MOFs with more complicated internal geometries. One example from a recent experiment is shown in Fig. 8.

4.4. Relationship between glass and furnace temperature

The glass temperature T_{glass} for each experiment is calculated via Eq. (18). The difference between the glass and furnace temperature is expressed as a percentage of furnace temperature for the six experiments in Fig. 9. For each experiment this percentage difference is almost constant as the operational parameter is varied. For experiments 1, 2, 5 and 6 this percentage is 25–27%, and for experiments 3 and 4, where the tubular preforms with larger holes were used, the percentage is 30–31%. This is strong evidence that the difference between the glass and furnace temperatures is best accounted for with a multiplicative factor based on the preform geometry, rather than a subtractive offset determined by operational parameters as has been assumed previously [16]. The small amount of variation in the percentage offset throughout the course of each experiment is at least partly due to preform taper, which alters the thermal mass of the neck-down as the draw progresses.

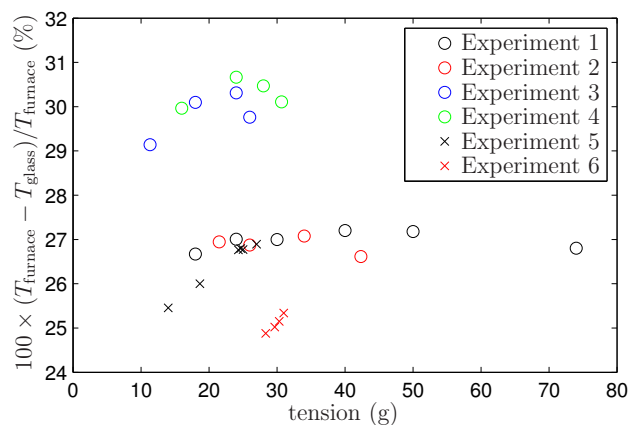


Fig. 9. Difference between measured furnace temperature and calculated glass temperature expressed as a percentage of furnace temperature for each experimental point. Note that for experiment 5 the relationship between draw speed and tension is given in Fig. 5(c) and for experiment 6 the relationship between pressurisation and tension is given in Fig. 6(c).

5. Conclusions

Six tubular preforms were drawn to fibre under a range of operational conditions. The comparison between the resulting fibres and the modelling predictions is extremely promising, despite the modelling consistently underestimating the observed geometry in several of the experiments. This discrepancy is revealing since the model predictions display the correct trend as fibre tension, for instance, is varied, thus suggesting that an important effect has been neglected from the modelling. A likely candidate for this effect is self-pressurisation which would, if present, account for the larger than predicted inner channel. Additionally, the experiment where the preform was actively pressurised showed good agreement with the modelling, although it appears that the apparatus which measures pressure in the draw tower may not be consistent with the pressure that is actually applied to the preform.

The magnitude of self-pressurisation for each observation was calculated and it was shown that self-pressurisation increases with tension or draw speed throughout each of the experiments. We hypothesise that the mechanism by which this occurs involves the magnitude of the pressure increasing with fibre tension.

There is evidence that the percentage difference between glass temperature and furnace temperature is constant, whereas previously the absolute difference between furnace and glass temperature was assumed to be constant. For the preforms with a larger diameter ratio this percentage was 30–31% and for the preforms with a smaller diameter ratio it was 25–27%.

Future work will include further modelling and experiments to investigate self-pressurisation. In particular this will focus on determining how this effect manifests in more complicated cross-sectional geometries where many channels are present.

Acknowledgments

This research was supported by grant DP130101541 from the Australian Research Council and by a Research Grant from the Leverhulme Trust in the United Kingdom. It was in part performed at the Optofab node of the Australian National Fabrication Facility utilising Commonwealth and SA State Government funding. We thank Jeremy Wong at the University of Adelaide for fibre geometry measurements.